Supporting Information

Yu et al. 10.1073/pnas.1109485108

SI Materials and Methods

Nano-Patterned Glass Substrate. Nano-imprint lithography was utilized to fabricate the physical barriers on glass substrates (1, 2). A silicon-based imprint mold was made by electron-beam lithography and anisotropic etching processes. Cover glasses (#1.5, Corning Inc., Corning, NY, USA) were first cleaned by Piranha solution (H_2SO_4 and H_2O_2 mixed in 3:1 ratio) for 15 min, rinsed with deionized (DI) water, and then spin-coated with UV-curable imprint polymers. Patterns were then transferred from the mold to the glass by high pressure stamping the imprint mold onto the polymer-coated cover glass and curing the polymer. After demolding, oxygen plasma etching was used to extend imprinted trenches vertically to the surface of the cover glass. A thin chromium metal layer was deposited by thermal evaporation and then the chromium outside the lines was selectively removed by resist lift-off processing. Typically, metal lines were 100 nm in width and 5 nm in height with a gap distance ranging from 4 μm to 500 nm.

Supported Lipid Bilayer Membranes. 1,2-dioleoyl-*sn*-glycero-3-phosphocholine (DOPC) and 1,2-dipalmitoyl-*sn*-glycero-3-phosphoethanolamine-N-(cap biotinyl) (16:0 biotinyl-Cap-PE) were purchased from Avanti Polar Lipids (Alabaster, AL, USA). Phosphate buffered saline (PBS), bovine serum albumin (BSA), and casein were purchased from Sigma-Aldrich (St. Louis, MO, USA)

Detailed preparation methods were previously described (3, 4). In brief, lipids with a desired composition were mixed in chloroform, and subsequently dried by a rotary evaporator. Mixed lipids were then hydrated with 2 mL of DI water over night. Small lipid vesicles, usually 100 nm in diameter, were made by 60 s probe-sonication in an ice bath, and then centrifuged at 20,000 x *g* for 4 h. 1 mL of supernate solution of small lipid vesicles was collected and stored at 4 °C. Before membrane deposition, glass substrates were cleaned by bath-sonication in 1:1 (Vol/Vol) isopropyl alcohol: water mixture for 30 min and rinsed with 100 mL DI water five times. Glass substrates were then exposed to intense deep-UV (185 nm) in an enclosed container for 30 min (Caution!! Avoid eye and skin exposure.), rinsed with 100 mL DI water five times, and dried under a clean nitrogen gas stream.

The lipids (0.4 mol% of biotinyl-Cap-PE and 99.6 mol% of DOPC) were mixed with an equal volume of 1x PBS, and then pipetted onto cleaned glass substrates for the self-assembly processes. Excess lipid vesicles were removed by immersing the entire glass substrate into a DI water bath. The lipid-coated glass substrate was then assembled with a Chamlide magnetic chamber (Live Cell Instrument, Seoul, Korea) within the water bath at room temperature. After assembly, supported lipid membranes in the chamber were always kept under aqueous conditions by immersing with 3 mL of solvent. In addition, supported lipid membranes and the nano-patterned substrates were blocked by incubation of 10 ~ 50 μg/mL of BSA or casein for 30 min. Excess blocking solution was removed by serial solvent exchange, 25 mL of 1x PBS in total for each chamber.

Membrane Functionalization. Cascade Blue and DyLight 633 conjugated neutravidin was purchased from Invitrogen (Carlsbad, CA, USA) and Thermo Fisher Scientific (Rockford, IL, USA), respectively. RGD-peptide, a biotinylated peptide of cyclo [Arg-Gly-Asp-D-Phe-Lys(Biotin-PEG-PEG)], was purchased from Peptides International (3697-PI, Louisville, KY, USA).

Neutravidin serves as the link between biotinyl-Cap-PE and biotinylated RGD-peptide (5). 1 μg/mL of fluorescently labeled neutravidin was added onto supported lipid membranes for 30 min in room temperature. Excess neutravidin was removed by serial solvent exchange, 25 mL of PBS in each chamber. Next, 1 μg/mL of biotinylated RGD was added to neutravidin-coated supported membranes for 30 min in room temperature. Excess RGD was removed by serial solvent exchange, 25 mL of 1x PBS in each chamber, and then 15 mL of serum-free DMEM media. Live cells were then added onto RGD-functionalized supported membranes within 2 h after preparation. Without RGD-peptide functionalization, cells failed to adhere to supported membranes (Fig. S4).

Based on quantitative fluorescence calibration (6), the surface density of biotinylated RGD linked by neutravidin on 0.4 mol% biotin-lipid membranes was approximately $1{,}750 \pm 400$ molecules/μm^2. However, the physical $x-y$ dimensions of neutravidin and integrin-α5β1 are about 5.4 nm × 5.8 nm (7), and 8 nm × 12 nm (8), respectively. Although one neutravidin could bind multiple biotinylated RGDs, single RGD-neutravidin units could only ligate with one integrin-α5β1 (or αvβ3), due to the limitation of their physical dimensions. Thus, the effective surface density of RGD, which was able to activate integrins, should be less than what we measured.

Cell Culture and Fluorescent Fusion Proteins. DMEM media, fetal bovine serum (FBS), penicillin, streptomycin, Hepes, TrypLE Express (trypsin-like proease), and Neon electroporation kits were purchased from Invitrogen (Carlsbad, CA, USA).

HeLa epithelial cells and MDCK epithelial cells were purchased from ATCC (Manassas, VA, USA). HeLa-JW epithelial cells with stable expression of paxillin-YFP were generous gifts from Dr. Zaidel-Bar R, Mechanobiology institute, Singapore (9). RPTP$^{+/+}$ fibroblasts were generous gifts from Dr. Sap JM, NYU, New York, NY, USA (10). Unless otherwise noted, all cells were grown in DMEM media supplemented with 10% (Vol/Vol) FBS, 100 U/mL penicillin, 100 μg/mL streptomycin, and 20 mM Hepes in 37 °C incubators with 5% CO_2. These cell types behaved similarly on RGD-membranes. Unless otherwise noted, HeLa cells were utilized to characterize lateral reorganizations of ligated integrin complexes. Fig. 4 and Fig. S7 are examples of MDCK cells. Typically, there are about 10^4 copies of αvβ3 per cell (11, 12).

Lifeact-Ruby constructs were generous gifts from Dr. Wedlich-Soldner R, Max Planck Institute of Biochemistry, Martinsried, Germany (13). Myosin regulatory light chain RFP (MLC-RFP) (14) and talin-EGFP (15) were from our previous work. Integrin-β3-EGFP constructs were generous gifts from Dr. Wehrle-Haller B, Center Médical Universitaire, Geneva, Switzerland (16). MLC-EGFP constructs were generous gifts from Dr. Ikebe M, University of Massachusetts, Worcester, MA, USA (17). Vinculin-EGFP constructs were gifts from Dr. Bershadsky AD, Weizmann Institute of Science, Rehovot, Israel and Mechanobiology institute, Singapore (18). FAK-EGFP constructs were gifts from Dr. Parsons JT, University of, Charlottesville, VA, USA (19). Electroporation was utilized to transiently transfect fusion constructs into cells, by the manufacturer's protocol. Cells were harvested by TrypLE Express after 18 to 24 h of transfections. To avoid nonspecific interaction from serums, cells were then resuspended in serum-free DMEM media in a 37 °C incubator with 5% CO_2 for 30 min before imaging.

Inhibition Chemicals. Blebbistatin, latrunculin A, and 4-amino-5-(4-chlorophenyl)-7-(t-butyl)pyrazolo[3,4-*d*]pyrimidine (PP2)

were purchased from Sigma-Aldrich (St. Louis, MO, USA). Chemicals were first dissolved in dimethyl sulfoxide (DMSO) with a stock concentration 1,000-times higher than the final concentration. Final concentrations were: blebbistatin 50 μM, latrunculin A 200 nM, PP2 10 μM. Before applying to cells, chemicals were diluted 1,000-times into DMEM media.

Microscopy and Data Analyses. Fluorescent images of live cells were taken by a spinning-disk confocal inverted microscope (PerkinElmer UltraVIEW VoX, Waltham, MA, USA), with 100x oil immersion lens (1.40 NA, UPlanSApo 100x, Olympus, Center Valley, PA, USA) and back-thinned electron multiplier CCD camera (C9100-13, Hamamatsu Photonics, Hamamatsu, Japan). An environmental chamber (37 °C and 5% CO_2) was attached to the microscope body for long-term time-lapse imaging. Acquired images were analyzed by ImageJ (NIH, Bethesda, MD, USA), Imaris (Bitplane AG, Zurich, Switzerland), and Matlab (MathWorks, Natick, MA, USA).

Within individual cells, clusters of ligated RGD-integrins and associated adaptor proteins were identified by Imaris under identical particle-searching criteria, including center position, area, intensity, and time point. These parameters for each cluster were then processed by a home-written Matlab code. Kymographs were generated by ImageJ.

The normalized intensity ratios between RGD-integrins (I_{RGD}) and associated adaptor proteins ($I_{\mathrm{EGFP\text{-}protein}}$) were calculated by the following procedure. Along each cluster trajectory, we first measured the fluorescence intensity with background subtraction at each cluster area, as Fig. 5 *A–D*. The series of intensity ratio ($I_{\mathrm{EGFP\text{-}protein}}/I_{\mathrm{RGD}}$) per unit area at each time point were then normalized within each trajectory. To compare the intensity ratio, the first time point of a newly detected integrin cluster was assigned to time zero. Normalized intensity ratios between each colocalized cluster of RGD-integrin and adaptor proteins were then plotted together, as Fig. 5*E*.

1. Guo LJ (2004) Recent progress in nano-imprint technology and its applications. *Journal of Physics D: Applied Physics* 37:R123.
2. Fengxiang Z, Hong Yee L (2006) Ordered three-dimensional hierarchical nanostructures by nano-imprint lithography. *Nanotechnology* 17:1884–1890.
3. Lin W-C, Yu C-H, Triffo S, Groves JT (2010) Supported membrane formation, characterization, functionalization, and patterning for application in biological science and technology. *Current Protocols in Chemical Biology* 2:235–269.
4. Yu CH, Groves JT (2010) Engineering supported membranes for cell biology. *Medical & biological engineering & computing* 48:955–963.
5. Nair PM, Salaita K, Petit RS, Groves JT (2011) Using patterned supported lipid membranes to investigate the role of receptor organization in intercellular signaling. *Nat Protocols* 6:523–539.
6. Salaita K, et al. (2010) Restriction of receptor movement alters cellular response: physical force sensing by EphA2. *Science* 327:1380–1385.
7. Hendrickson WA, et al. (1989) Crystal structure of core streptavidin determined from multiwavelength anomalous diffraction of synchrotron radiation. *Proceedings of the National Academy of Sciences* 86:2190–2194.
8. Nermut MV, Green NM, Eason P, Yamada SS, Yamada KM (1988) Electron microscopy and structural model of human fibronectin receptor. *The EMBO journal* 7:4093–4099.
9. Zaidel-Bar R, Milo R, Kam Z, Geiger B (2007) A paxillin tyrosine phosphorylation switch regulates the assembly and form of cell-matrix adhesions. *J Cell Sci* 120:137–148.
10. von Wichert G, et al. (2003) RPTP-alpha acts as a transducer of mechanical force on αv/β3-integrin-cytoskeleton linkages. *The Journal of cell biology* 161:143–153.
11. Benedetto S, et al. (2006) Quantification of the expression level of integrin receptor αvβ3 in cell lines and MR imaging with antibody-coated iron oxide particles. *Magnetic Resonance in Medicine* 56:711–716.
12. Zhang X, et al. (2006) Quantitative PET Imaging of Tumor Integrin αvβ3 Expression with 18F-FRGD2. *J Nucl Med* 47:113–121.
13. Riedl J, et al. (2008) Lifeact: a versatile marker to visualize F-actin. *Nat Meth* 5:605–607.
14. Tamada M, Perez TD, Nelson WJ, Sheetz MP (2007) Two distinct modes of myosin assembly and dynamics during epithelial wound closure. *The Journal of cell biology* 176:27–33.
15. Zhang X, et al. (2008) Talin depletion reveals independence of initial cell spreading from integrin activation and traction. *Nature cell biology* 10:1062–1068.
16. Ballestrem C, Hinz B, Imhof BA, Wehrle-Haller B (2001) Marching at the front and dragging behind. *The Journal of cell biology* 155:1319–1332.
17. Komatsu S, Yano T, Shibata M, Tuft RA, Ikebe M (2000) Effects of the regulatory light chain phosphorylation of myosin II on mitosis and cytokinesis of mammalian cells. *The Journal of biological chemistry* 275:34512–34520.
18. Zamir E, et al. (1999) Molecular diversity of cell-matrix adhesions. *J Cell Sci* 112:1655–1669.
19. Tilghman RW, et al. (2005) Focal adhesion kinase is required for the spatial organization of the leading edge in migrating cells. *J Cell Sci* 118:2613–2623.

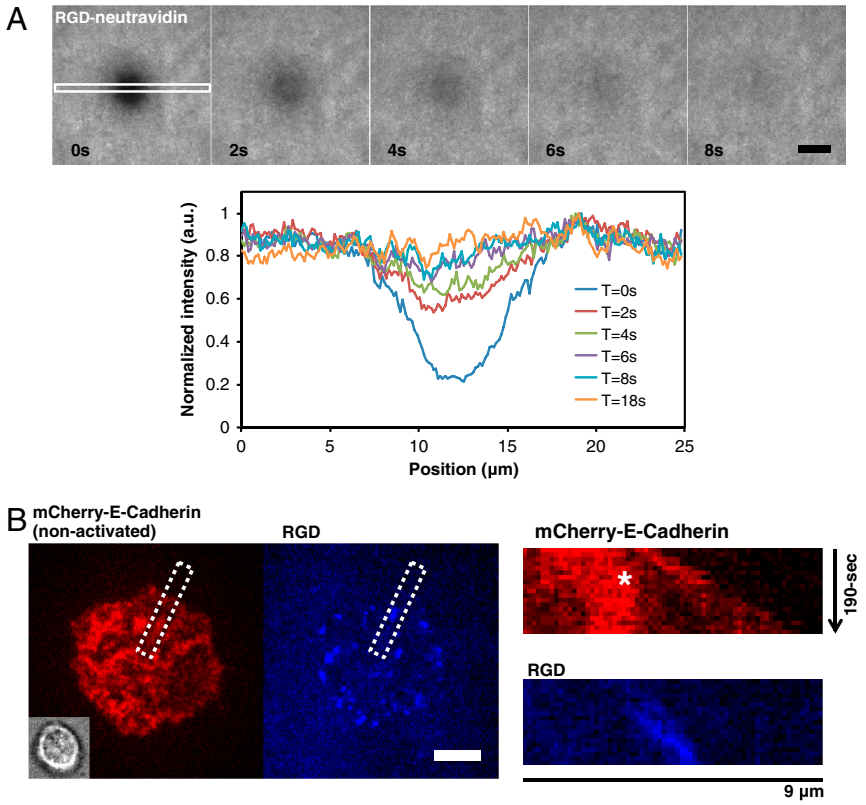

Fig. S1. (*A*) Lateral mobility of RGD-functionalized supported lipid membranes. RGD peptides were linked to the supported membrane via DyLight 633 neutravidin. Fluorescence recovery after photo-bleaching (FRAP) demonstrates lateral mobility of RGD-functionalized supported lipid membranes. The central dark spot in the first image ($t = 0$) was taken immediately after photo-bleaching, and there was complete recovery within 18 s. The normalized intensity plot (bottom) indicates the recovery of fluorescent intensities within the white box at various time points. The calculated diffusion coefficient was approximately 2.5 $\mu m^2/s$. (Scale bar, 5 μm). (*B*) Kymograph of nonactivated mCherry-E-Cadherin in plasma membrane and RGD-integrin clusters (upper-right and lower-right box, respectively) were taken from the selection region in a spreading cell (boxes in the left boxes). While both RGD-integrin clusters and cell membrane moved out, nonactivated E-cadherin was stationary (while aster). This observation indicated there was no biased outward movement of bulk membranes during the early adhesion phase. Previously, Gauthier, et al. (1) also demonstrated that exocytosis of lipid vesicles does not occur in the early phase of cell spreading. (Scale bar, 5 μm).

1 Gauthier, et al. (2011) Temporary increase in plasma membrane tension coordinates the activation of exocytosis and contraction during cell spreading. *Proc Natl Acad Sci USA.* 108:14467–14472.

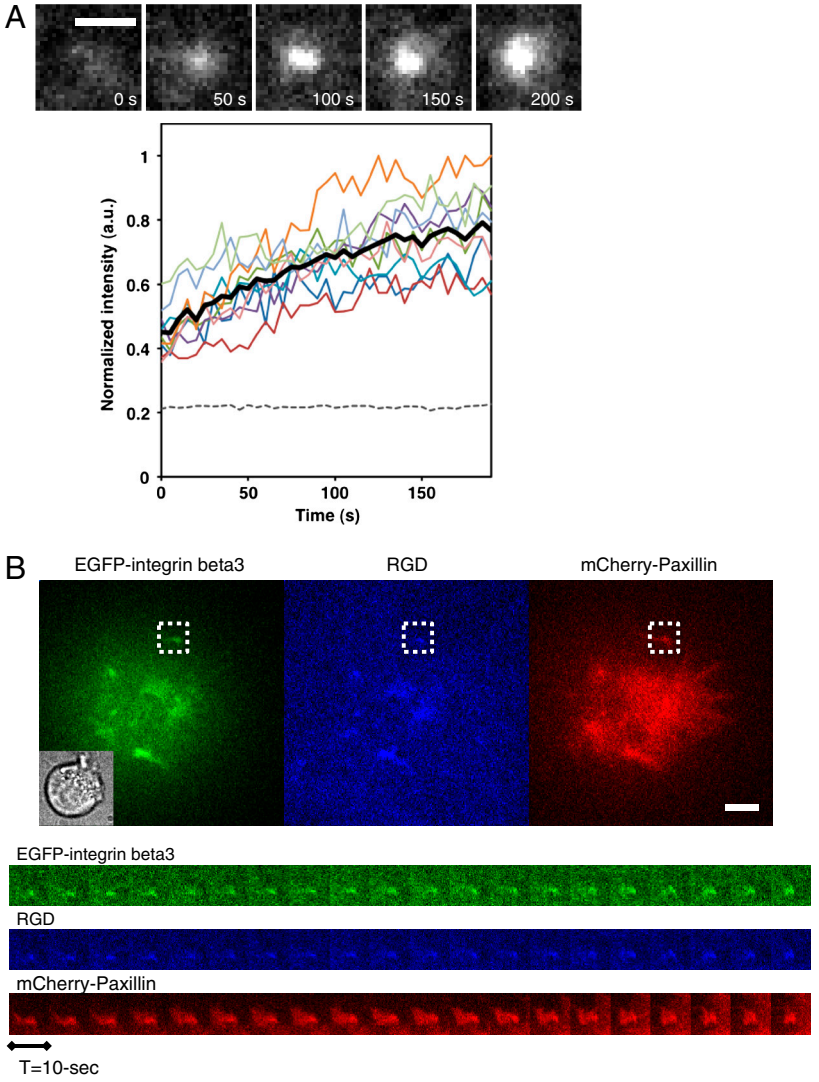

Fig. S2. (*A*) Monotonically increasing fluorescence intensity of RGD-integrin clusters during the early phase of cell adhesion. Gray dashed line represents background intensity of RGD-neutravidin over the area with no cells and shows no significant photo-bleaching within 200 s. Local intensity maximum of individual RGD-integrin clusters was measured and then normalized (colored thin lines). The bold line represented averages of normalized nine trajectories. (Scale bar, 2 μm). (*B*) Colocalization of RGD, EGFP-integrin beta3, and mCherry-Paxillin in live cells. As RGD clusters grow, integrin beta3 are promptly localized with the clusters, with Pearson correlation coefficient 0.73 (RGD and beta3). Concurrently, paxillin are also recruited, due to activated integrin beta3. (Scale bar, 5 μm) and 10 s each frame.

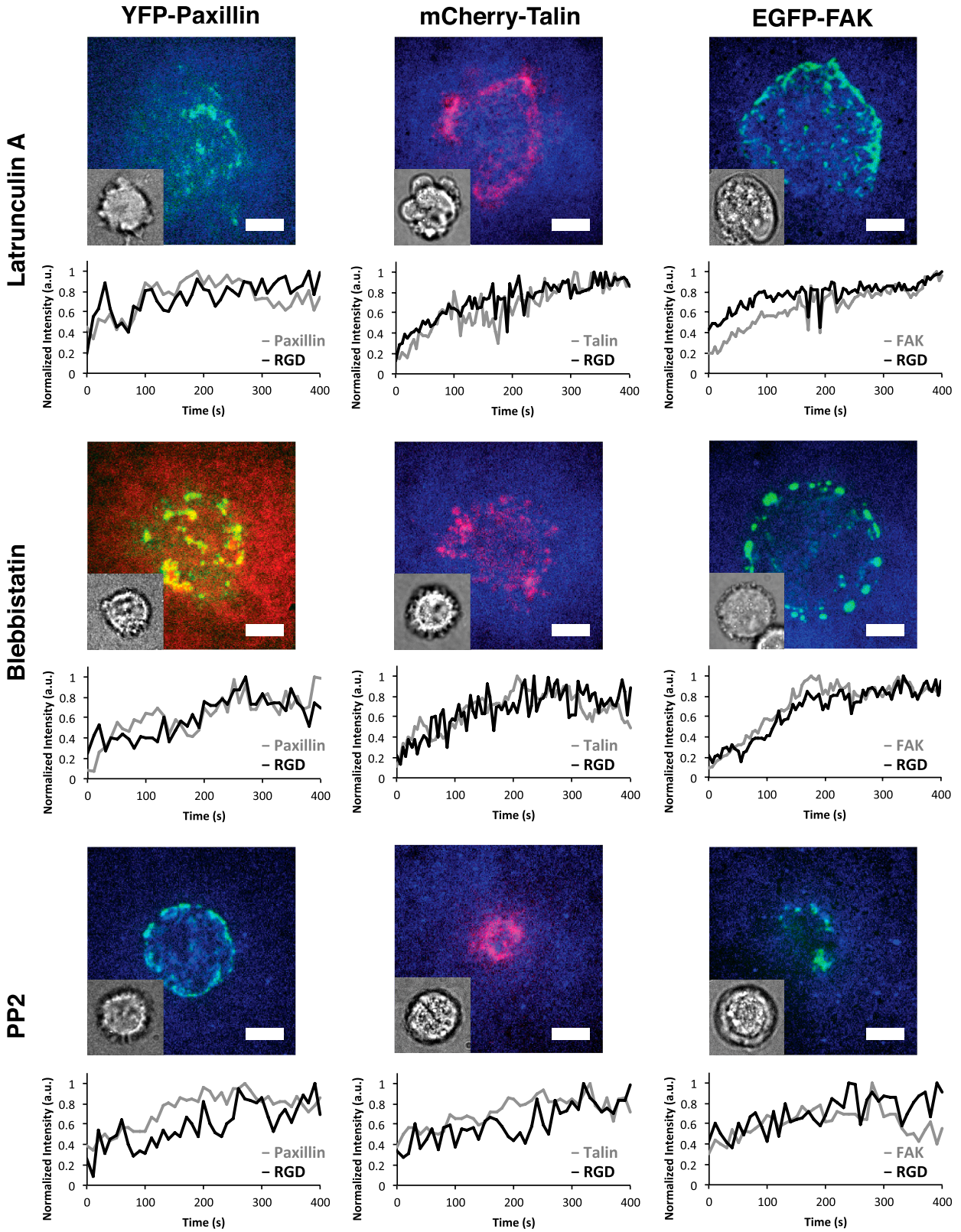

Fig. S3. Association of talin, paxillin, and FAK with RGD/integrin clusters in the early phase of cluster formation, following pretreatment with the inhibitors, latrunculin A (200 nM), blebbistatin (50 μM), and PP2 (10 μM). RGD-integrin clusters were able to nucleate, but usually lacked collective movement. RGD-peptide was labeled by far-red neutravidin (DyLight 633 conjugated, in the box of YFP-paxillin and blebbistatin) or Cascade Blue neutravidin (the rest). Normalized intensity of clusters over time, including YFP-paxillin, mCherry-Talin, and EGFP-FAK, were measured by the same calculation in Fig. 5. Because clustering of RGD reports on the ligation and clustering of integrin beta 3, the simultaneous clustering of these adaptor proteins shows that they are recruited in the early phase of RGD-integrin clustering. We observed smaller clusters with these inhibitors. (Scale bar, 5 μm).

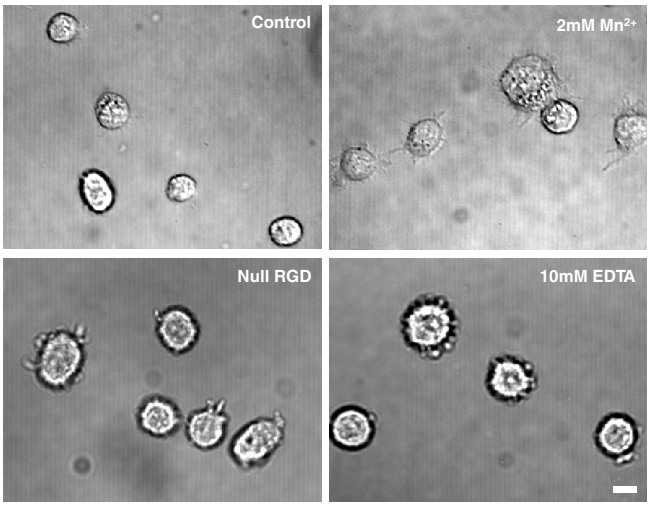

Fig. S4. Specific RGD-integrin mediated cell adhesion. Cells fail to adhere onto both EDTA-treated and null-RGD-supported membrane with line barriers (2 μm gap spacing). However, cells are able to adhere to RGD-supported membrane under Tris buffer saline with 2 mM of manganese chloride within 20 min. (Scale bar, 10 μm).

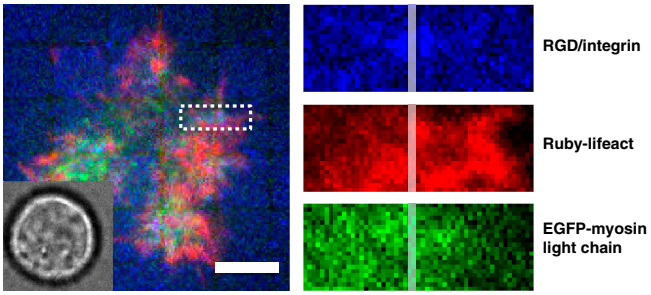

Fig. S5. In the early cell adhesion, both actin and myosin between contractile integrin/RGD clusters were observed. As actin remodeling occurs around the cluster, actomyosin network is often structureless and diffusive among newly formed clusters. Scale bar 5 μm and gap spacing is 4 μm.

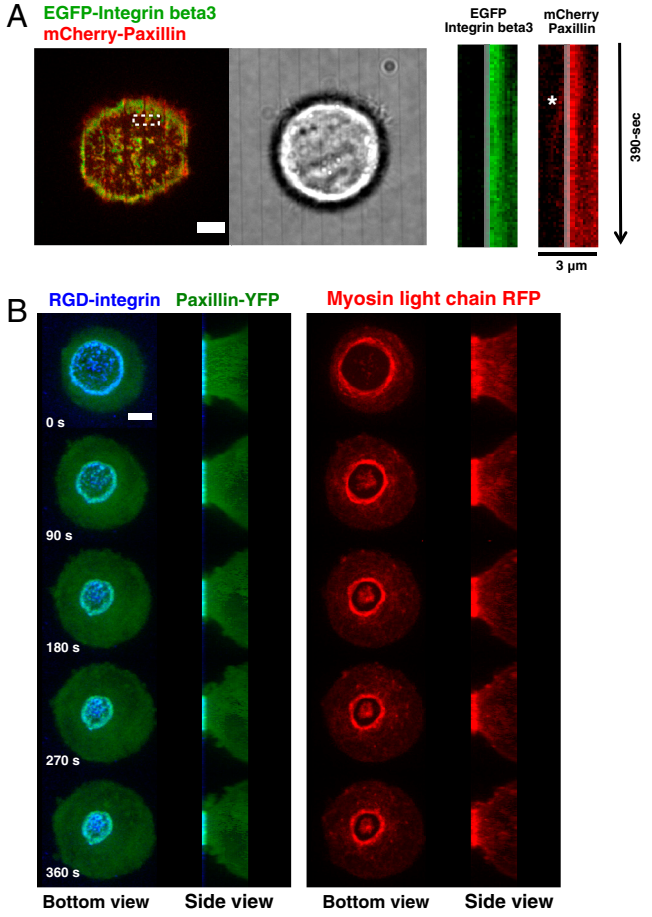

Fig. S6. (*A*) EGFP-integrin beta3 stay besides the barriers as the cell starts to contract. Paxillin could be pulled away and dissociated from integrin/RGD complex (while aster in the kymograph of paxillin), possibly due to greater force mediated by myosin-II during retraction phase. Kymographs of both integrin beta3 and paxillin were taken in the selected region of the cell on patterned RGD-supported membranes (boxed region in the left box). Scale bar 5 μm and gap spacing 4 μm. (*B*) Inward movements of ligated integrin complexes were mediated by myosin retraction. Time-lapsed confocal images of RGD, paxillin-YFP, and MLC-RFP revealed three-dimensional (3D) redistributions of cytoskeletal proteins and cell morphology. During the retraction phase, myosins formed contractile mesh-like cortical actomysin networks and moved ligated integrins and paxillins inwards. As a result, the cell formed a contractile ring that lifted up the rest of the cell in a nearly spherical morphology. Confocal *z* setting was 500 nm each step, and total 20 steps. 3D reconstruction was rendered by ImageJ. See Movie S3. (Scale bar, 5 μm).

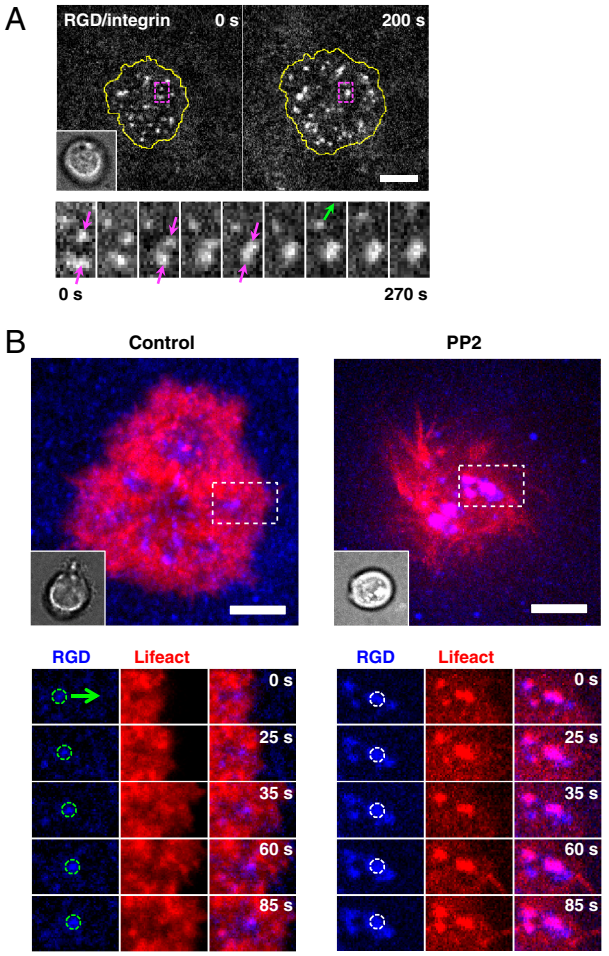

Fig. S7. (*A*) Initial contractile movements of ligated integrin clusters occasionally occurred on continuous RGD-supported membranes, and were essential for following cell spreading processes. The same cell was shown in Fig. 4*A*. The stable contractile pair of ligated integrin clusters could serve as local anchoring points for outward polymerization of actin that drove adjacent clusters moving out. (Scale bar, 5 μm). (*B*) Outward movement of ligated integrin complexes and accompanied actin lamellipodial protrusion (left box). Pretreatment of 10 μM PP2 did not inhibit RGD-integrin cluster growth, but clusters lacked lateral mobility (right box). No lamellipodial spreading was observed. Actin filaments were localized to RGD-integrin clusters and assembly was not observed in surrounding areas. (Scale bar, 5 μm).

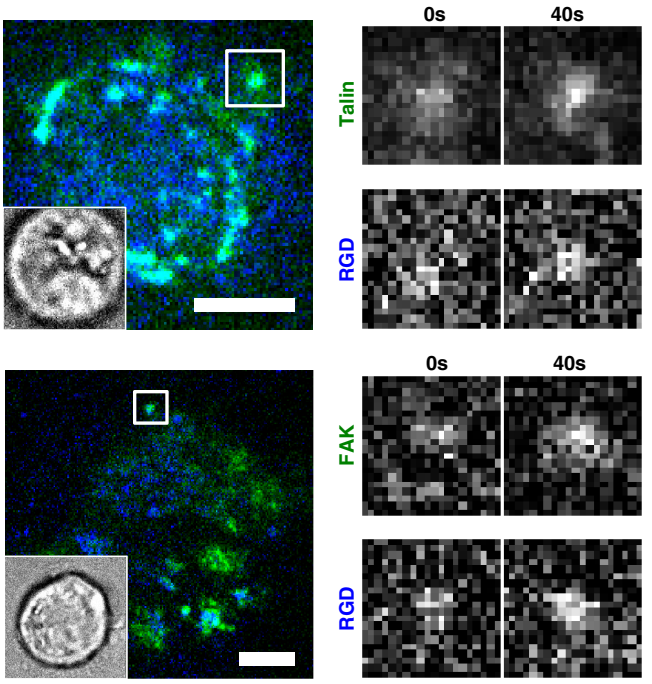

Fig. S8. EGFP-talin (top) and EGFP-FAK (bottom) associations at RGD-integrin clusters (labeled by Cascade Blue) during the early adhesion formations. Both talin and FAK were promptly recruited at newly formed integrin clusters. (Scale bar, 5 μm).

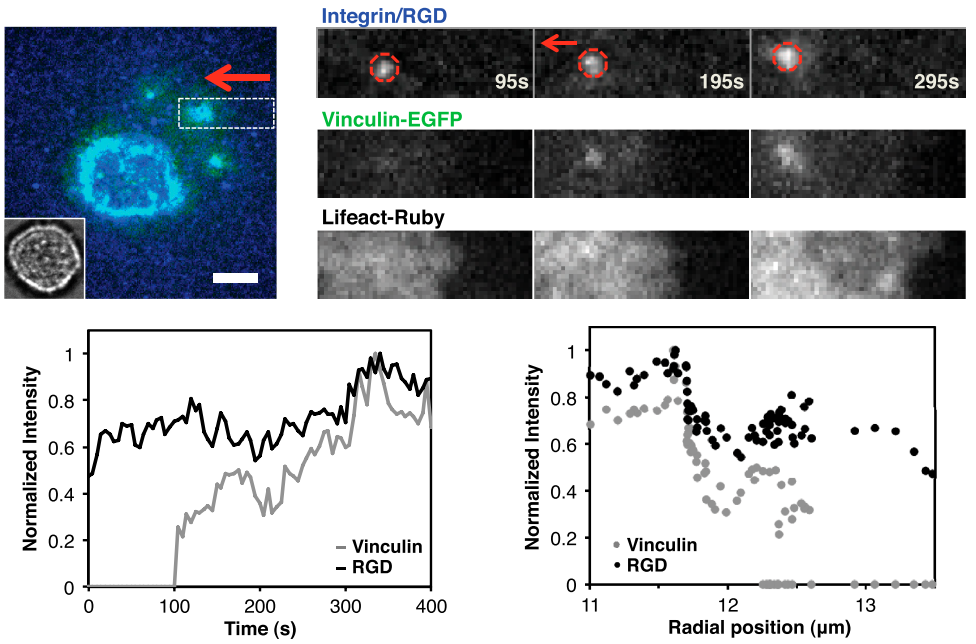

Fig. S9. Normalized intensity plot (bottom left) was taken from Fig. 5*B*. Initially, vinculins (green) were not actively associated at RGD-integrin clusters (blue). As the cluster moved inwards during the retraction phase, vinculins were then recruited at the ligated integrin complexes. The box in the bottom right represented increased vinculin association at RGD-integrin clusters as moving inwards. Thus, vinculin recruitment was modulated by higher level of inward retraction force. (Scale bar, 5 μm).

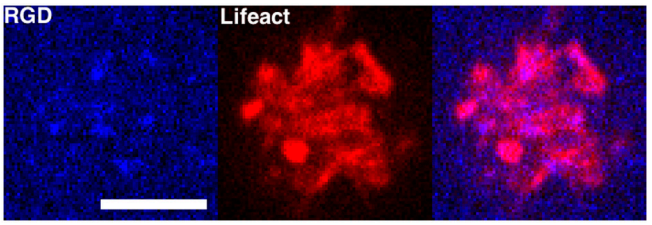

Movie S1. Nucleation of RGD-integrin clusters causes actin network remodeling and stimulates actin polymerizations in proximity during the initial cell adhesion. Within initial 100 s, actins (Ruby-Lifeact) were firstly enriched at the newly formed RGD-integrin cluster sites and then started active expansion around RGD-integrin clusters. Video was taken every 3 s and played as six frames per second. (Scale bar, 5 μm).

Movie S1 (MOV)

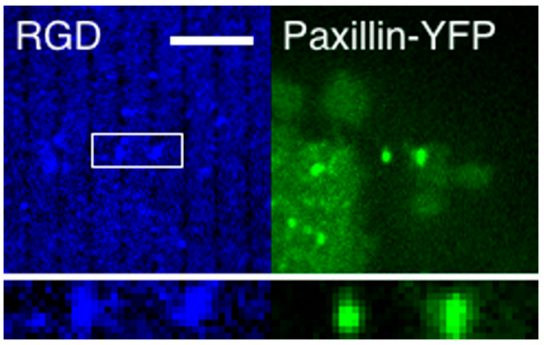

Movie S2. Formation of contractile pair assembly during initial adhesion. Contractile pair assembly of ligated RGD-integrin clusters across nano-patterned metal lines during initial adhesion. RGD-integrin clusters and associated paxillin-YFP laterally move towards each other and pile up against the physical barrier of metal lines. Bottom boxes were boxed regions from the top boxes. Video was taken every 5 s and played as three frames per second. (Scale bar, 5 μm).

Movie S2 (MOV)

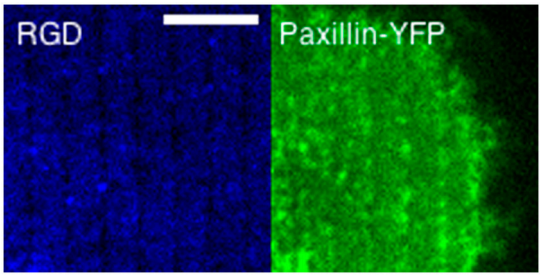

Movie S3. Active cell spreading and subsequent retraction on nano-patterned RGD-membranes. Video was taken every 10 s and played as 18 frames per second. Selected kymographs were shown in Fig. 3*B*. (Scale bar, 5 μm).

Movie S3 (MOV)

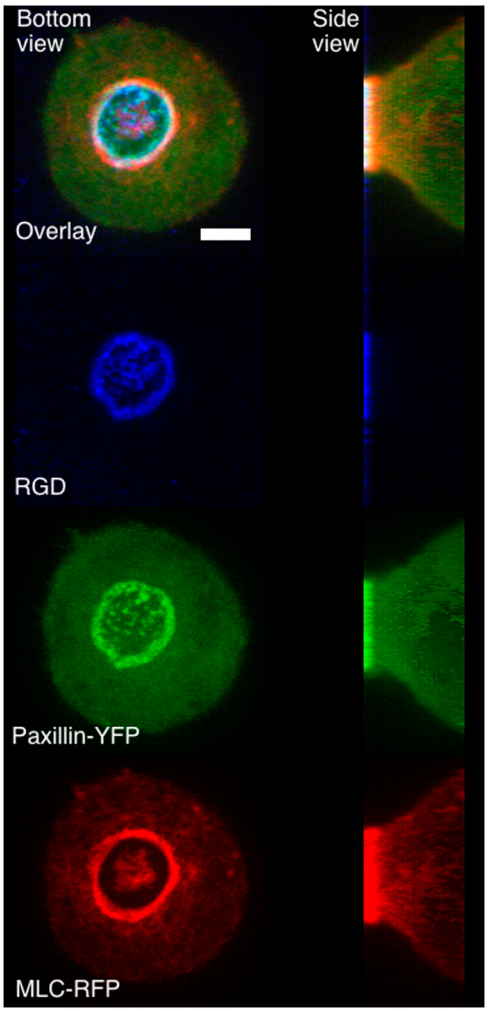

Movie S4. Live cell confocal time-lapsed images of Fig. S6*B*. Inward movements of ligated integrin complexes were mediated by myosin activities. Time-lapsed confocal images of RGD (blue), paxillin-YFP (green), and MLC-RFP (red) revealed 3D redistributions of cytoskeletal proteins and cell morphology. During the retraction phase, myosins formed contractile mesh-like cortical actomysin networks and moved ligated integrins and paxillins inwards. As a result, the cell formed a contractile ring that lifted up the rest of the cell in a nearly spherical morphology. Confocal *z* setting was 500 nm each step, and total 20 steps. 3D reconstruction was rendered by ImageJ. Video was taken every 30 s and played as three frames per second.

Movie S4 (MOV)

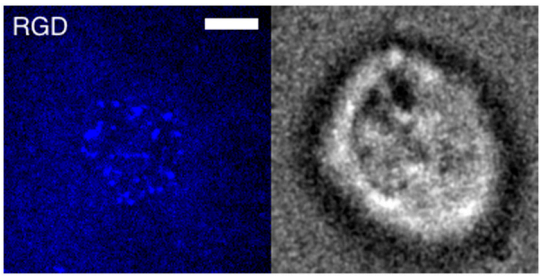

Movie S5. Long-ranged lateral movement of integrin clusters. During cell spreading, ligated integrin clusters firstly moved outwards and then inwards. Video was taken every 30 s and played as six frames per second. (Scale bar, 5 μm).

Movie S5 (MOV)